Grain Morphology and Trapping Effects on Electron Transport in Dye-Sensitized Nanocrystalline Solar Cells

M. J. Cass,[†,‡] Alison B. Walker,[*,†] D. Martinez,[†] and L. M. Peter[§]

Department of Physics and Department of Chemistry, University of Bath, Bath BA2 7AY, United Kingdom

Received: July 2, 2004; In Final Form: November 17, 2004

We have examined the combined effects of grain morphology and electron trapping on the transient response of photoelectrons moving through the TiO_2 grains in a dye-sensitized nanocrystalline solar cell using a multi-time-scale random walk Monte Carlo model. Our use of a multi-time-scale approach enables us to simulate transport for electrons moving through spherical connected grains in a three-dimensional (3D) voided network and look at the effect of the size of interparticle boundaries on carrier dynamics. We can also address similar times to those over which measurements are taken, namely, 0.1 ms. These times are long because of deep traps in the TiO_2 grains. The grains have 2-fold connectivity in one dimension (linear chains) or 4-fold or 6-fold connectivity in three dimensions and traps with an exponential distribution of energies. Photoelectrons are generated by a light pulse of short duration. The spatial distribution of the photogenerated electron density from this pulse either has a uniform profile or is peaked on the electrolyte side. We show that the constrictions at the grain necks slow the electrons, making trapping more likely and hence further delaying their passage to the extracting electrode. By comparing our results for 4-fold and 6-fold coordinated particles on a cubic lattice with 2-fold coordinated particles on linear chains, we show that transport is slowed in the former case due to the additional paths available to the electrons in the 3D network. We also find that the charge and current transients cannot be fit to an analytical solution of the continuum equations with an effective diffusion coefficient even at long times. Therefore, caution must be exercised when attempting to fit experimental transient data with an effective diffusion coefficient.

1. Introduction

Dye-sensitized nanocrystalline solar cells (Grätzel cells) show great promise, giving energy conversion efficiencies exceeding 10% and performing well under indirect radiation, yet are composed of low-cost materials.[1,2] The active absorber is a monolayer of ruthenium-based dye adsorbed onto a film comprising grains of TiO_2. Electrons travel through this film to the collecting contact. By providing a model that considers (i) electron motion inside and between grains, (ii) the effects of grain necks on slowing electron transport, (iii) grains linked as linear chains and on a three-dimensional (3D) network, (iv) traps, and (v) extraction, we can see how these effects in combination influence the photocurrent. We show how competition between diffusion to the extracting electrode along the pathways determined by the connectivity of the grains, removal at the extracting electrode, and slowing down due to trapping exacerbated by the grain necks determines the transient response. Our main conclusion is that all the effects listed above are important. Our results have implications for the time taken to reach a photostationary state. As this time can be long, assumptions often made in interpreting transient measurements that electrons achieve a photostationary state may be invalid.

Many studies[3,4] have shown that electron transport in the TiO_2 grains occurs by diffusion since the fields across the film are screened by the electrolyte and the small size of the particles does not support a built-in field.[5] Trapping and detrapping of the electrons influences strongly the transit time for electrons across the films as demonstrated by large amplitude transient photocurrent and photovoltage measurements[6,7] and intensity modulated photocurrent and photovoltage data.[8−14] The characteristic response time for the cells is sensitive to the illumination intensity I_0, being several minutes at very low light levels and milliseconds at solar illumination intensities.[11,15] As I_0 increases, more electrons are injected into the TiO_2 grains, filling the deep traps, so that the remaining electrons are less likely to be trapped in deep traps and reach the extracting electrode more quickly.

The concentration and energetic distribution of traps in the TiO_2 film are difficult to control whereas the morphology of the film is influenced by fabrication methods.[16,17] Thus, it is important to determine how the morphology affects electron transport to identify ways of improving the efficiency of the cell. Park et al.[8] used intensity-modulated photocurrent and scanning electron microscopy to compare rutile and anatase TiO_2 films in solar cells and showed that electron transport is slower in rutile films. They argue that this can be explained from fewer interparticle connections in the rutile structure, leading to a reduced number of pathways to the electrodes.

Many Monte Carlo simulations have already been made on the electron density dependence of charge transport.[15,18−21] To produce a simulation that can be run on a reasonable time scale, one approach[18,22] is to assume that the time electrons spend untrapped is negligible in comparison to the time spent trapped, and thus electrons move directly between traps. The problem with this approach is that the distances between the traps are

* Corresponding author. E-mail: a.b.walker@bath.ac.uk.
† Department of Physics.
‡ Present address: Department of Chemistry, SBMS, The University of Surrey, Guildford, Surrey GU2 7XH, United Kingdom.
§ Department of Chemistry.

10.1021/jp047073f CCC: $30.25
Published on Web 02/25/2005

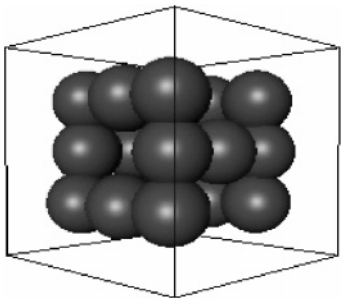

Figure 1. The grain connectivity in the 3D network.

very hard to calculate for a realistic morphology, and so it is hard to discern the influence of the morphology. Furthermore, Jakobs and Kehr[23] have pointed out that this approach is mainly relevant to cases where the probability of tunneling to an adjacent site is similar to the probability of thermal emission to the conduction band, for example, in highly doped materials or at low temperatures, and Nelson et al.[22] have concluded that the alternative approach of a multiple trapping model is a better representation of recombination kinetics and, we would infer, of electron transport. In a multiple trapping model, the electrons execute a random walk while in the conduction band, and their progress is interrupted by a series of trapping and detrapping events. On detrapping, they return to the conduction band.

In other Monte Carlo simulations,[18,22] electrons have been confined to lattice sites for simple cubic geometries. Here and in ref 10, we have adopted a much more realistic geometry in which electrons move through sintered spherical grains connected by necks of varying width. In ref 10, we showed that trapping and morphology affect the transport properties of a film by means of Monte Carlo simulations of electron motion through linear chains of TiO_2 grains using a novel two time scale approach. For this paper, we have extended this approach to include a morphology that more accurately approximates the structure of a nanocrystalline film. The grain centers are placed on a voided three-dimensional (3D) cubic lattice, as shown in Figure 1 and described in section 2, such that each grain is connected to four others since it has been shown that a coordination of four is the most probable.[9,24] Use of a cubic coordination simplifies the calculation enormously.

A recent study on the effects of film geometry[9] has shown that the diffusion coefficient deduced from transient current data varies strongly with the porosity (the ratio of the volume occupied by the pores to that of the grains) and has explained these results with a Monte Carlo simulation of electron hopping on a random nanoparticle network. This study looked at films with porosities varying from 55%, a typical value for films used in solar cells, to porosities near the percolation limit of 76%. Our simulated film porosities typify those for measured nanocrystalline films (less than 60%) and are below the percolation limit, so there is an infinite cluster on which the particles can move and percolation is not a limiting factor. We thus argue that percolation theory on its own is not sufficient to explain the slow electron transport. For comparison, we also present some results where grains are positioned at all sites on a simple cubic lattice, thus giving 6-fold coordination.

Two sets of initial conditions are employed, both representing a short-lived pulse of illumination just before the transients are measured. With a short-lived pulse, the injected electrons do not have time to fill the traps in the TiO_2 grains prior to the start of the simulation. First, we look at spatially uniform illumination causing in turn a spatially uniform distribution of photogenerated charge density. This corresponds to illumination wavelengths for which the absorption length (the inverse of the absorption coefficient) significantly exceeds the cell width. Second, we examine sheet illumination, in which a sheet of charge is generated at the electrolyte side of the film. This scenario corresponds to ultraviolet (UV) light illumination of film from the electrolyte side, because UV can excite electrons across the TiO_2 band gap in addition to exciting dye molecules. This leads to an absorption length orders of magnitude shorter than the device width, so excitation is confined to grains closest to the counter electrode. Use of UV light to measure the transient response via D_{eff} for different conditions (e.g., the amount of dye adsorption) in dye-sensitized cells has attracted attention recently.[29]

As a measure of the transient response, we have used the charge transients, which measure the charge extracted from the cell at a given time, in preference to the transient photocurrents reported in ref 10 because the latter are noisy at long times because of the small number of electrons. To find out if our data can be characterized by fitting a value of D_{eff}, we obtained analytical solutions for the continuity equation in which the traps and morphology are represented solely through D_{eff}. Earlier work on multiple trapping models[23] has shown that the transient currents for a distribution of trap energies display dispersive behavior in which the transient current does not decay with time in the extraction regime as a power law. Such power law behavior is seen in our work on dye-sensitized cells with traps at a single energy[10] when the transient currents can be fitted to a model with a well-defined D_{eff} value. Here, we have assumed trap energies that tail off into the band gap with an exponential distribution in accordance with experimental observations[12,13] and found that it is impossible to obtain a unique value for D_{eff}. Our work also agrees with that of de Jongh and Vanmaekelbergh,[26] who showed that the dispersive regime cannot be characterized by a single transit time, which is equivalent to the lack of a unique value for D_{eff}.

For simplicity, back reactions have been neglected. Electron−electron interactions are largely screened out by the ions in the electrolyte and by the large static dielectric constant (∼30) of TiO_2[25] and so are ignored here. They are unlikely in any case to be important at solar intensities that correspond to a few electrons being injected per grain. An exception could be for sheet illumination at short times where there could be a large number of electrons per grain in the grains on the electrolyte side. However, the electron concentration rapidly evens out between the grains, and so any electron−electron interactions would only be noticeable at short time scales that are obscured by the RC time constants of the cell.

The outline of our paper is as follows: section 2 describes the network morphology and how the Monte Carlo method is extended beyond ref 10; section 3 describes our predicted results for the time dependence of the extracted charge Q for both uniform and sheet illumination; section 4 concludes. An appendix provides the analytical solution for sheet illumination within the continuum model.

2. Method

A system of coordinates is adopted such that the x axis is normal to the electrodes and $x = 0$ is positioned at the extracting electrode. We have considered two geometries, a linear chain system with 2-fold coordination and a 3D network on simple cubic lattice sites. For 6-fold coordination, grains are positioned at all the sites. To achieve 4-fold coordination, one in four lattice sites is left unoccupied. A given grain has nearest neighbors on the y and z axes but not on the x axis, on the x and z axes but

TABLE 1: Grain Densities for the Chosen Neck Angles

α_{neck} (rad)	grain density (m^{-3})
0.12558	9.6×10^{22}
0.44779	1.28×10^{23}
0.66413	1.92×10^{23}

not on the *y* axis, or along the *x* and *y* axes but not along the *z* axis. The three coordinations can be obtained from each other by rotations through 90°. Hence, the list of possible outcomes can be generated by only one type of coordination, and the results for the other type of coordination can be obtained by rotations. Periodic boundary conditions were implemented in the *y* and *z* directions, where, to avoid the complication of added rotations as electrons cross the boundaries, an even number of grains is used in the *y* and *z* directions.

For both the linear chains and the 3D network, for the different neck sizes the grain separation in the chain system is adjusted so that all of the chain systems have a given grain density. For the chains, the number of grains in each chain is adjusted so that each chain has a chosen thickness. A similar procedure is applied to the 3D network except here only the number of grains in the *x* direction is adjusted.

The density of TiO_2 grains will depend on the size of the overlap. In the chain system the density required is obtained by varying the separation between chains. In the 3D system, the grain density is given by

$$\rho = \frac{0.75}{(2r\cos(\alpha_{neck}))^3} \tag{1}$$

The factor of 0.75 is a result of only three in four of the cubic lattice sites being occupied by a grain since each grain is connected to only four neighbors, leaving empty sites on the cubic lattice.

Consequently, for grains of a given radius the grain density depends only on the neck size. If the density of traps is to be kept constant, then the number of traps per grain must be adjusted when changing the neck size. Since there can only be an integer number of traps per grain, this means the neck sizes examined must be chosen with care when comparing results for different grain densities. The grain densities selected are given in Table 1. These values are chosen so that a range of neck sizes are investigated, and the grain densities are in a simple ratio ($^1/_2$:$^1/_3$:$^1/_4$); thus to have the same density of traps in each film, the number of traps per grain is taken in the proportion to the grain density. So, for example, a density of 3.84×10^{23} traps m^{-3} is achieved in the system with 0.126 rad necks by including four traps per grain and in the case of 0.664 rad necks by including two traps per grain. To compare the linear chain system with this system, the same values of neck size are used in both cases.

2.1. Monte Carlo Simulations. To enable us to look at electron motion through the grain network on time scales of 0.1 ms, with the simulation time scale $t_{scatter}$ of 2 fs, we have divided the simulation into two time scales as described in ref 10. In the linear chains, the grains are all interchangeable except those close to the ends of the chains. Consequently, in general the probabilities of an electron moving a given number of grains toward or away from the contact are the same. In the 3D network, we can generate one set of probabilities, for example, an electron starting on an *x*-connected grain, and make the appropriate rotation for an electron starting on a *y*- or *z*-connected grain.

We must also assess whether the new location falls within the cross section of a trap. Traps are assigned locations within a cuboid that contains the grain, excluding the overlap regions. For example, if the grain has four necks in the *y* and *z* directions

$$x_{trap} = 2r_{grain}\mathscr{R} \tag{2}$$

$$y_{trap} = 2(r_{grain}\cos(\alpha_{neck}))\mathscr{R} \tag{3}$$

$$z_{trap} = 2(r_{grain}\cos(\alpha_{neck}))\mathscr{R} \tag{4}$$

where $\mathscr{R}$ is a random number between 0 and 1. We then test the new location; if the selected point falls outside the grain, then it is reflected back into the grain. This is done by moving the trap to the surface of the grain along a line joining its position outside the grain to the grain center. Thus, the probability of finding a trap is higher at the surface of the grain than in the grain interior. Reference 22 indicates that the electrolyte influences the density of trap states, so it seems likely that traps are more common at or near the surface of the grains.

Whenever an electron is less than a trap radius from the trap center, it is recorded as an encounter with a trap, and the walk continued. This procedure enables us to deal with the case when the trap encountered is already full in the coarse scale simulation.

With the list of possible outcomes from the fine scale simulation, we can carry out a coarse scale simulation of electrons moving through the TiO_2 film. The boundary conditions were as follows. The grains nearest the counter electrode are considered to be perfectly reflecting. In all cases except the results in Figure 8, the extracting electrode is treated as being a perfect sink. For Figure 8, a given fraction of the electrons reaching the extracting electrode are reflected, and the rest are extracted.

Trap energies are chosen using

$$E_T = \frac{k_B T}{\beta}\ln(\mathscr{R}) \tag{5}$$

where E_T is the energy of the trap relative to the conduction band edge E_C (so $E_T < 0$) and β is a measure of the width of the distribution, such that the larger β is, the greater the likelihood of shallow traps.

The trap may initially be occupied by an intrinsic electron with a probability

$$f(E_T) = \frac{1}{1 + \exp((E_{Fdark} - E_T)/k_B T)} \tag{6}$$

where E_{Fdark} is the dark Fermi level relative to E_C (so $E_{Fdark} < 0$). From the occupancy probability, we determine whether the trap is filled for the duration of the simulation by generating a random number. If this number is less than *f*, then the trap is permanently filled; if not, then it begins the simulation empty. If a full trap is encountered, then the step is redone using the probabilities for electrons moving after encountering one trap.

When an electron does become trapped, the time it remains trapped depends on the trap energy via

$$\tau_r = \frac{1}{N_c \upsilon_{th}\sigma}\exp\left(\frac{E_T}{k_B T}\right) \tag{7}$$

where τ_r is the trap residence time, N_c is the density of states in the conduction band, and υ_{th} is the electron thermal velocity.

3. Results and Discussion

Below, we have used the parameter values in Table 2 except where stated otherwise.

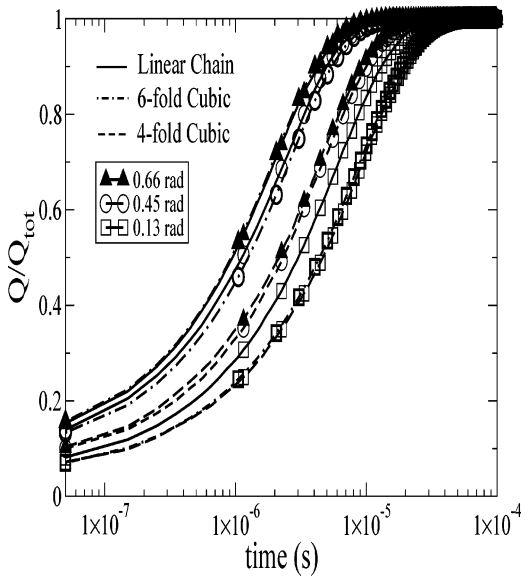

Figure 2. Comparison between total charge extracted Q as a ratio of injected charge Q_{tot} with no traps present for linear chains with 2-fold coordination (solid lines), and a cubic network with 6-fold coordination (chained lines) and 4-fold coordination (dashed lines) and in grains with neck angles of 0.66 rad (filled triangles), 0.45 rad (empty circles), and 0.13 rad (empty squares). An electron density is assumed of 3.84×10^{23} m^{-3}, corresponding to 4 electrons/grain.

TABLE 2: Fixed Parameter Values

parameter	value
temperature T	300 K
trap distribution width β	0.2
cell width d	2 μm
grain radius r_{grain}	10 nm
time step (fine scale)	2 fs
time step (coarse scale)	0.2 ns

TABLE 3: Effective Diffusion Coefficients for Trap Free Chain (1D) and 4-Fold Coordinated Cubic (3D) Systems Fitted Using Results Shown in Figure 2

system	α_{neck} (rad)	$t_{1/2}$ (μs)	D_{eff} (m^2 s^{-1})
1D	0.66	0.953	8.0×10^{-7}
1D	0.44	1.14	6.8×10^{-7}
1D	0.13	3.04	2.6×10^{-7}
3D	0.66	2.15	3.7×10^{-7}
3D	0.44	2.31	3.4×10^{-7}
3D	0.13	4.65	1.7×10^{-7}

3.1. Uniform Illumination. In this section, we consider the transient response when the initial density of photogenerated charge is constant across the cell.

Figure 2 shows the effect of intergrain neck size and grain coordination on the rate of charge extraction in the absence of traps. Table 3 shows the values of $t_{1/2}$, the time taken for half the injected charge to escape the film, and D_{eff} deduced from $Q(t)$ shown in Figure 2. The main conclusion to be drawn from Figure 2 is that if the intergrain necks are large, then the transport of electrons is faster and transport slows as the coordination changes from 2-fold coordination (i.e., linear chains) to 6-fold and then to 4-fold coordination in the cubic networks. If α_{neck} is 0.66 rad, then Q is almost identical for the 2-fold and 6-fold networks but much slower for the 4-fold network. Similarly, if α_{neck} is 0.45 rad, then the rate of charge extraction is close for the 2-fold and 6-fold coordination but noticeably slower for the 4-fold cubic network. However, if α_{neck} is 0.13 rad, then the charge is extracted faster for the 2-fold coordination, and there is little difference between the 6-fold and 4-fold cubic networks.

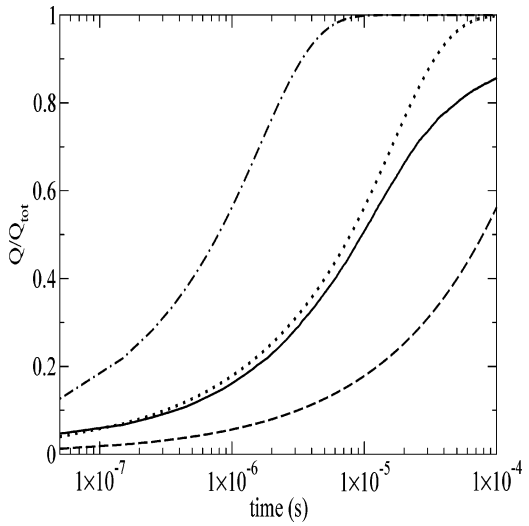

Figure 3. Total charge extracted Q as a ratio of injected charge Q_{tot} for a 3D network and a trap concentration and electron density each being 3.84×10^{23} m^{-3} in grains with narrow necks (0.13 rad), corresponding to 4 traps per grain. Monte Carlo simulations (solid line) are compared with analytical solutions for $D_{eff} = 1 \times 10^{-6}$ m^2 s^{-1} (chained line), 1×10^{-7} m^2 s^{-1} (dotted line), and 1×10^{-8} m^2 s^{-1} (dashed line).

For a linear system, Table 3 shows that the response time $t_{1/2}$ is approximately three times slower for $\alpha_{neck} = 0.13$ rad than that for $\alpha_{neck} = 0.44$ rad as compared to a factor of 2 slow for the 4-fold coordinated 3D system. For linear chains, as the necks become larger, the value of $t_{1/2}$ will tend toward the value obtained for diffusion in a cylinder. At low neck sizes, the same pattern is followed for the 4-fold cubic system. In this case, however, as the neck size increases above 0.3 rad, $t_{1/2}$ levels out and stays approximately constant thereafter.

The reason for the above observations is that in linear chains the electrons move only up and down the chain. The electrode is therefore reached in a much shorter time than in the 3D systems where electrons can take more tortuous paths, especially in the 4-fold coordinated system where the reduced coordination makes it even less likely than for the 6-fold coordinated system that the electrons can reach the electrode in a given time. As the neck size increases for a given film thickness, the number of grains in the x direction increases, thus enhancing the number of possible necks through which the electrons have to traverse on each path and the number of paths available to them (eq 1). This effect compensates to some extent for the easier passage due to the wider necks.

When traps are introduced, they slow the progress of electrons. We have chosen trap and electron concentrations to be comparable to experimental measurements at intensities $\approx$ solar intensities.[10] The shape of the transients differs from curves that can be obtained from the analytical solution in refs 11 and 27 by varying D_{eff} as can be seen in Figure 3. Consequently, a unique value of D_{eff} cannot be obtained, and $t_{1/2}$ is a better measure of the response time than D_{eff}. This is because the processes of trapping and detrapping within the grain morphology are not adequately represented by the continuity equation with all the trapping and slowing down at the grain necks folded into D_{eff}. In ref 10, we were able to find values of D_{eff} for linear chains with a trap at a single energy (0.3 eV below E_C) by fitting the analytical solutions to the transient photocurrent by eye. Nevertheless, we observed that the transients from solutions of the continuity equation representing transport in a quasi-homogeneous medium differed noticeably from the Monte Carlo predictions. This was true even when traps were explicitly

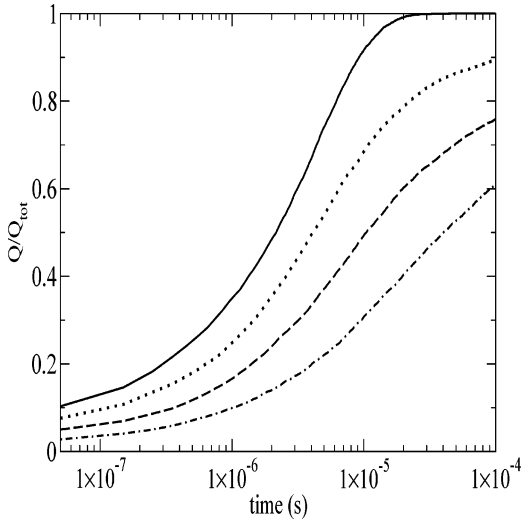

Figure 4. Extracted charge Q as a ratio of injected charge Q_{tot} for a 3D network and trap densities of 3.84×10^{23} m^{-3} (dotted line), 7.68×10^{23} m^{-3} (dashed line), and 11.52×10^{23} m^{-3} (chained line), corresponding respectively to 2, 4, and 6 traps per grain. The grains have wide necks (0.66 rad), and the electron density is 3.84×10^{23} m^{-3}, i.e., 2 electrons per grain from Table 1.

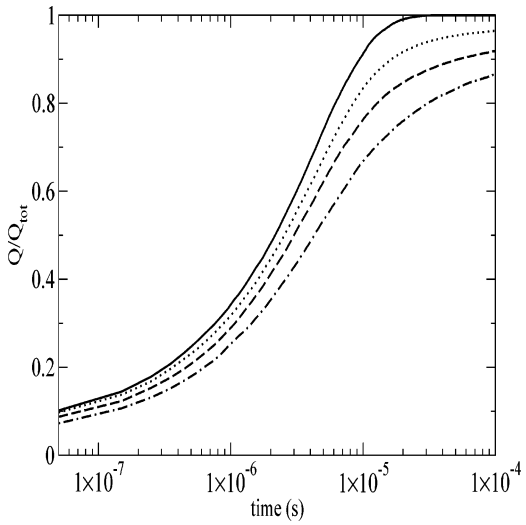

Figure 5. As for Figure 4 but for an electron concentration of 11.52×10^{23} m^{-3}, i.e., 6 electrons per grain.

included in the continuity equations, and a numerical solution was found in place of the analytical solution in refs 11 and 27. Here, we find that the additional complications of a 3D network and a trap distribution are sufficient to rule out D_{eff} as a useful parameter for characterizing the transients; thus dispersive behavior is observed.

The electron concentration relative to the trap concentration is important as we show in Figures 4 and 5. If the electron concentration is lower than the trap concentration, as in Figure 4, then electrons will generally encounter empty traps; hence almost all the electrons are slowed by trapping. If on the other hand the initial concentration of electrons exceeds the concentration of traps as in Figure 5, then some of the electrons fill the traps, leaving the rest free to move as though there were few or no traps. At short times, when the electron concentration is high, the presence of traps has little influence, and it is only at longer times when the electron concentration falls that trapping becomes more important. As we can see from Figure 5, when the initial electron concentration is greater than the trap concentration, $t_{1/2}$ changes little with trap concentration,

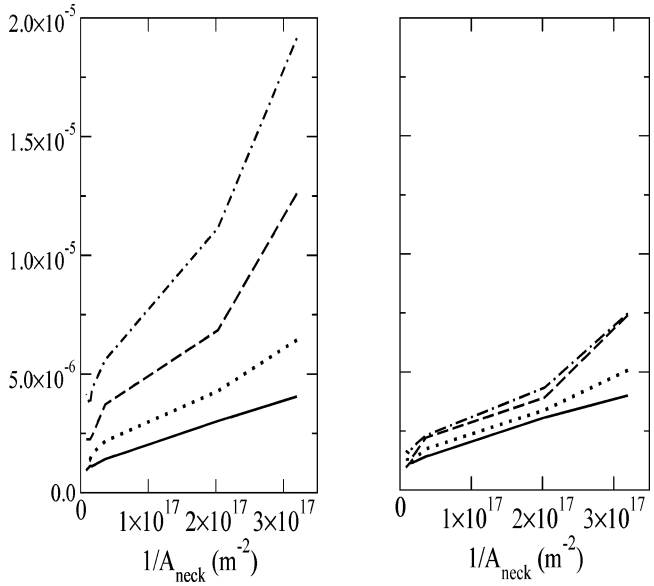

Figure 6. Variation of $t_{1/2}$ with the reciprocal of the neck area for a 1D linear chain and trap densities of 3.84, 7.68, and 11.52×10^{23} m^{-3} and an electron density of 3.84×10^{23} m^{-3} (left panel) and 11.52×10^{23} m^{-3} (right panel) in grains with narrow necks.

suggesting that the trap-filled limit has been reached. The first half of the photogenerated electrons to exit mostly encounter filled traps. In Figure 4, we can see that in contrast when the trap concentration exceeds the electron concentration $t_{1/2}$ varies greatly with trap concentration.

We can see how the introduction of traps to the system is affected by electron slowing down at the necks. Figure 6 shows the variation of $t_{1/2}$ with neck size as measured by $1/A_{neck}$, which is approximately linear as would be expected. Results are given for the 1D linear chain since in the 3D systems we would only be able to obtain three points due to the need to use comparable concentrations. In the right-hand panel of Figure 6, the gradient of the relationship is nearly constant and is fairly insensitive to the trap density, indicating that the trap-filled limit has been reached. However, the left-hand panel shows that the gradient is increasing with $1/A_{neck}$ and with the trap density, indicating that the size of the necks has a greater effect on transport as the number of traps increases. The reason for this is that as the neck size decreases the likelihood of an electron transferring from grain to grain is reduced; thus the likelihood of it encountering each trap within the current grain is increased. Thus, the effects of small necks and high trap concentrations reinforce each other.

The conclusion that small necks and trapping reinforce each other is confirmed in Figure 7 where we look at the number of times electrons are trapped in systems with different neck sizes. For large necks, there is a larger proportion of electrons trapped only a few times, and a much smaller proportion trapped 10 000 times or more than small necks. This is consistent with the notion that the narrower neck constrictions force the electrons to spend more time in the grains rather than being extracted. These calculations were also made for a 3D 4-fold coordinated network[28] but are not shown here as they give similar conclusions and so we merely note the point that the electrons in a 3D network encounter many more traps than in the 1D network as there are substantially more paths to reach the extracting electrode and these paths are longer.

All of the previous results were generated for thin (2 μm) TiO_2 films. The necks slow transport, so the thicker the film, the more necks which must be passed, and hence the more

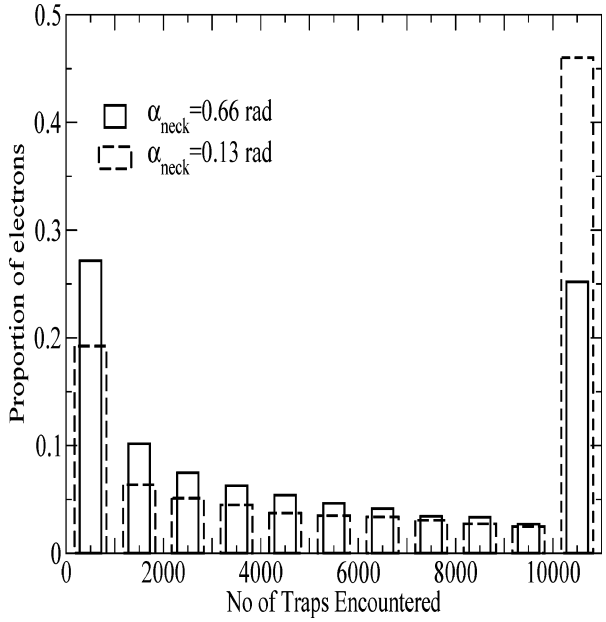

Figure 7. The number of times electrons trap for a 1D linear chain as a fraction of the total number of electrons in the system for 0.66 rad necks (solid line) and 0.13 rad necks (dashed line) with trap and electron concentrations each of 3.84×10^{23} traps m^{-3}. The bars on the furthest right indicate the number of electrons trapping 10 000 times or more.

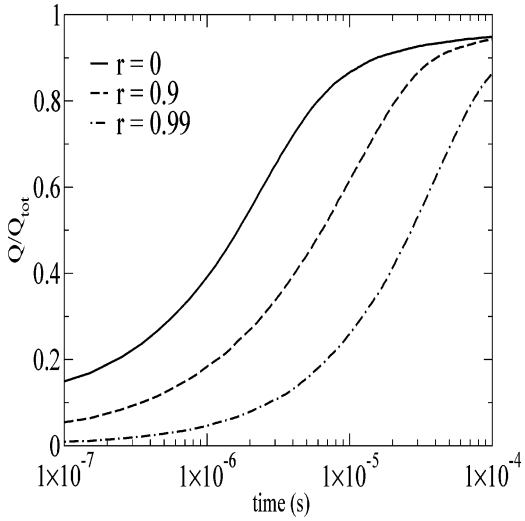

Figure 8. Charge transients for barriers with reflectivities of 0, 0.9, and 0.99 for a 1D linear chain and thickness of 2 μm, with 0.45 rad necks and trap and electron concentrations each of 3.84×10^{23} traps m^{-3}.

noticeable the effect of slowing down by necks. It has been shown[28] that if Q/Q_{tot} is plotted against t/d^2, then the curves coincide as would be expected from random walk theory.

It is also possible that there might be a barrier to the extraction of charge once it has reached the extracting electrode. It is simple to incorporate this effect into the model as explained in section 2 by reflecting the electron a fixed fraction of the times it attempts to exit the film. Figure 8 shows that the contact must be almost entirely reflecting in order to have a significant impact on the transport.

3.2. Sheet Illumination. Motivated by recent measurements of transient photocurrents, such as those in ref 29, we have investigated the simulated transient charge for the initial condition of sheet illumination at the electrode side of the film.

When there are no traps present, it is possible to find a unique D_{eff} by fitting eq 13 to the transients for $Q(t)$. Our results are given in Table 4 for linear chains (1D) and 3D systems. These results show that $t_{1/2}$ is longer and D_{eff} less than the values obtained for uniform illumination (Table 3), suggesting that transport for sheet illumination is slower. The same trends can be seen in Table 3, namely, that electrons take longer to leave the cell in the 3D system than in the 1D system and for the narrower necks.

TABLE 4: Fitted Values of D_{eff} and Deduced Values for the Extraction Time $t_{1/2}$ for Sheet Illumination[a]

system	α_{neck} (rad)	$t_{1/2}$ (μs)	D_{eff} (m^2 s^{-1})
1D	0.66	1.9	2.7×10^{-7}
1D	0.44	2.2	7.0×10^{-7}
1D	0.13	3.7	8.0×10^{-7}
3D	0.66	4.0	1.9×10^{-7}
3D	0.44	4.1	3.7×10^{-7}
3D	0.13	8.0	3.9×10^{-7}

[a] Here, $n_0 = 3.84 \times 10^{23}$ m^{-3} and narrow necks (0.13 rad) were used.

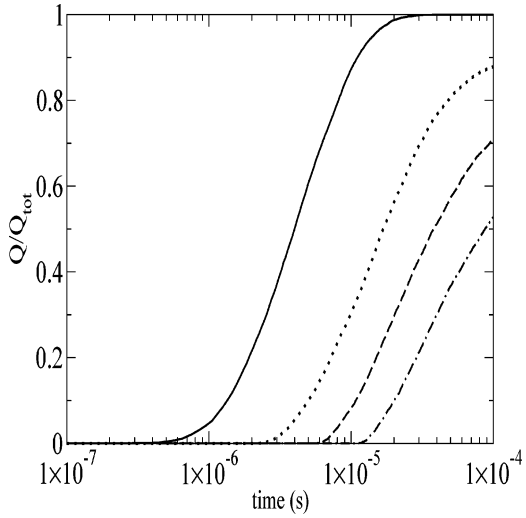

Figure 9. Here, the extracted charge as a ratio of the total charge is shown for a 3D network with 0.66 rad necks an electron density of 3.84×10^{23} m^{-3} (i.e., 2 per grain) and trap densities of 0 (solid line), 3.84×10^{23} m^{-3} (dotted line), 7.68×10^{23} m^{-3}(dashed line), and 11.52×10^{23} m^{-3} (chained line).

The effect of traps on $Q(t)$ and hence $t_{1/2}$ can be seen for different trap concentrations in Figure 9. The electron concentration is less than or equal to the trap concentrations so that we are below the trap-filled limit. Comparisons can be made with Figure 4, which shows the equivalent results for uniform illumination. The charge takes a while to start coming out of the extracting electrode since it takes a while to cross the film, but when it does, it comes out faster for the sheet illumination for a given trap density, corresponding to larger transient currents. For sheet illumination unlike uniform illumination, all of the electrons that reach the extracting electrode experience multiple trapping events. It is also clear from Figure 9 that the effect of trapping is much greater as one might expect given that all of the electrons have to traverse the film thickness in this case.

Qualitative conclusions from our simulations of the photocurrent $j(t)$ in ref 28 are the same as those that can be drawn from the transient currents in ref 29, namely, that when there is more trapping (in ref 29 this is because of an increased film thickness or lower bias light intensity resulting in unfilled traps) the peak in $j(t)$ occurs at later times, its magnitude drops, and it becomes more rounded. However, with traps in the system, the charge transients have a very different time dependence from

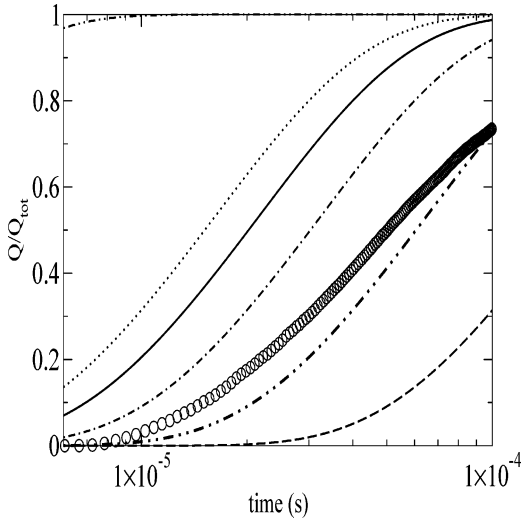

Figure 10. Total charge extracted Q as a ratio of injected charge Q_{tot} for a 3D network and a trap concentration and electron density each being 3.84×10^{23} m^{-3} in grains with wide necks (0.66 rad), corresponding to 2 traps per grain and 2 electrons per grain. Monte Carlo simulations (circles) are compared with analytical solutions for $D_{eff} = 1 \times 10^{-8}$m^2 s^{-1} (dashed line), 2.5×10^{-8} m^2 s^{-1} (chained line, 2 dots), 5×10^{-8} m^2 s^{-1} (chained line, 1 dot), 7.5×10^{-8} m^2 s^{-1} (solid line), 1×10^{-7} m^2 s^{-1} (dotted line), and 1×10^{-6} m^2 s^{-1} (chained line, 2 dots, top left of graph).

those predicted by the analytical solution in eq 13 as can be seen in Figure 10.

4. Conclusions

The transport of electrons in TiO_2 grains has been simulated over experimentally measured time scales. We find that the morphology of the TiO_2 film has a considerable impact on the transport of electrons through the film. By comparing results for a 3D network with 4-fold and 6-fold coordination with 1D linear chains, we find that the morphology can influence the rate at which electrons are extracted. The reason is that in the 3D network with 4-fold coordination electrons take more tortuous paths than those in the 6-fold coordinated network or linear chains. This affects the number of necks that the electrons have to traverse en route to the extracting electrode and their chances of being trapped.

The effects of morphological factors, such as the size of intergrain necks, cannot easily be separated from those of traps as the effects interact. Narrowing the intergrain necks results in greater trapping of electrons. The effect of intergrain necks on $t_{1/2}$ is roughly inversely proportional to the area of the intergrain neck. As the trap concentration increases so does the effect of the necks. An effective diffusion coefficient D_{eff} can be found by fitting the charge transients to analytical expressions but only in the absence of traps. When traps are present, the competition between slowing down due to trapping and extraction of charge at the extracting electrode provides transients that are quite different in shape to the analytical solutions and so a D_{eff} cannot be fitted. This suggests that care must be taken when using D_{eff} as a measure of the speed of the transient response, especially when simple expressions based on bulk diffusion are used.

We have also investigated sheet illumination, in which electrons are all generated close to the electrolyte side of the film. A delay is seen before the extracted charge starts to come out of the film, but once it starts coming out, it does so faster than for uniform charge generation. Whether a uniform or sheet illumination is used as the initial condition, the same trends with trapping and morphology as for uniform illumination are observed.

Acknowledgment. This work was supported by the U.K. Engineering and Physical Sciences Research Council.

Appendix: Analytical Solutions to the Continuity Equation

To see whether our predicted charge transients can be characterized by an effective diffusion coefficient D_{eff}, we have obtained analytical solutions to the continuity equation for the conduction electron density in the absence of recombination. We have assumed the electron density at $t = 0$ is determined by illumination that generates a total photogenerated charge per unit area $Q_{tot} = qn_0d$, where q is the magnitude of the electron and d is the cell thickness, and that no illumination is present from time $t = 0$, so that

$$\frac{\partial n}{\partial t} = D_{eff}\frac{\partial^2 n}{\partial x^2} \tag{8}$$

where x is the distance from the extracting electrode.

The extracting electrode boundary condition assumed here to permit an analytical solution is

$$n(x = 0, t) = 0 \tag{9}$$

This boundary condition corresponds to diffusion-limited electron collection; i.e., all the electrons reaching the extracting electrode by diffusion are extracted. It differs from the boundary condition for the extracting electrode adopted in numerical solutions of the continuity equation obtained in ref 10. At the electrolyte side, as in ref 10 we assume

$$\left.\frac{\partial n(x, t)}{\partial x}\right|_{x=d} = 0 \tag{10}$$

Two initial conditions are considered. First, uniform illumination resulting in a constant spatial distribution of photogenerated charge density

$$n(x, 0) = n_0 \tag{11}$$

Equation 8 has been solved analytically[11,27] for this case.

Second, we look at sheet illumination, i.e., a spatially peaked photogenerated charge density on the electrolyte side for as in the uniform case

$$n(x, 0) = n_0 d\delta(x - d) \tag{12}$$

The total photogenerated charge per unit area extracted at time t is

$$\frac{Q(t)}{Q_{tot}} = 1 - \frac{4}{\pi}\sum_{k=0}^{\infty}\frac{(-1)^k}{2k+1}\exp\left(\frac{-D_{eff}(2k+1)^2\pi^2 t}{4d^2}\right) \tag{13}$$

The photocurrent density

$$j(t) = \mathrm{d}Q(t)/\mathrm{d}t \tag{14}$$

In practice, all but the first term in the sum over k can be neglected in eq 13; thus we predict an exponential decay of the form $j(t) \propto \exp(-t/\tau)$ where $\tau = 4d^2/(\pi^2 D_{eff}) = d^2/(2.47D_{eff})$. Reference 29 obtained a different expression for $j(t)$ by assuming that there is a short pulse of illumination at $t = 0$ that

corresponds to a delta function in time but otherwise are solving the same problem (although it may be noted that eq 10 is not satisfied by their solution). D_{eff} was deduced by fitting $j(t)$ to an exponential decay, giving $\tau = d^2/(2.35D_{\text{eff}})$.

References and Notes

(1) Grätzel, M. *Nature* **2003**, *421*, 586.

(2) Nazeeruddin, M. K.; Péchy, P.; Renouard, T.; Zakeeruddin, S. M.; Humphry-Baker, R.; Comte, P.; Liska, P.; Cevey, L.; Costa, E.; Shklover, V.; Spiccia, L.; Deacon, G. B.; Bignozzi, C. A.; Grätzel, M. *J. Am. Chem. Soc.* **2001**, *123*, 1613.

(3) Peter, L. M.; Vanmaekelbergh, D. In *Advances in Electrochemical Science and Engineering*; Alkire, R. C., Kolb, D. M., Eds.; Wiley-VCH: Weinheim, Germany, 1999.

(4) Duffy, N. W.; Fisher, A. C.; Fulian, Q.; Peter, L. M.; Walker, A. B.; Wijayantha, K. G. U. In *Photovoltaics for the 21st Century*, Proceedings of Photovoltaics 2001−10, Washington, DC, Spring 2001; Kapur, V. K., McConnell, R. D., Carlson, D., Caesar, G. P., Rohatgi, A., Smith, J., Eds.; The Electrochemical Society: Pennington, NJ, 2001.

(5) Gregg, B. A. *J. Phys. Chem. B* **2003**, *107*, 4688.

(6) Trupke, T.; Würfel, P.; Uhlendorf, I. *J. Phys. Chem. B* **2000**, *104*, 11484.

(7) Wang, H.; He, J.; Boschloo, G.; Lindström, H.; Hagfeldt, A.; Lindquist, S. *J. Phys. Chem. B* **2001**, *105*, 2529.

(8) Park, N. G.; van de Lagemaat, J.; Frank, A. J. *J. Phys. Chem B* **2000**, *104*, 8989.

(9) Benkstein, K. D.; Kopidakis, N.; van de Lagemaat, J.; Frank, A. J. *J. Phys. Chem. B* **2003**, *107*, 7759.

(10) Cass, M. J.; Qiu, F. L.; Walker, A. B.; Fisher, A. C.; Peter, L. M. *J. Phys. Chem. B* **2003**, *106*, 113

(11) Duffy, N. W.; Peter, L. M.; Rajapakse, R. M. G.; Wijayantha, K. G. U. *Electrochem. Commun.* **2000**, *2*, 262.

(12) Duffy, N. W.; Peter, L. M.; Rajapakse, R. M. G.; Wijayantha, K. G. U. *Electrochem. Commun.* **2000**, *2*, 658.

(13) van de Lagemaat, J.; Frank, A. J. *J. Phys. Chem. B* **2000**, *104*, 4292.

(14) Dloczik, L.; Ileperuma, O.; Lauermann, I.; Peter, L. M.; Ponomarev, E. A.; Redmond, G.; Shaw, N. J.; Uhlendorf, I. *J. Phys. Chem. B* **1997**, *101*, 10281.

(15) Cao, F.; Oskam, G.; Meyer, G. J.; Searson, P. C, *J. Phys. Chem.* **1996**, *100*, 17021.

(16) Lindstrom, H.; Holmberg, A.; Magnusson, E.; Lindquist, S. E.; Malmqvist, L.; Hagfeldt, A. *Nano Lett.* **2001**, *1*, 97.

(17) Lindstrom, H.; Magnusson, E.; Holmberg, A.; Sodergren, S.; Lindquist, S. E.; Hagfeldt, A. *Sol. Energy Mater. Sol. Cells* **2002**, *73*, 91.

(18) van de Lagemaat, J.; Frank, A. J. *J. Phys. Chem. B* **2001**, *105*, 11194.

(19) Nelson, J. *Phys. Rev. B* **1999**, *59*, 15374.

(20) Kopidakis, N.; Schiff, E. A.; Park, N. G.; van de Lagemaat, J.; Frank, A. J. *J. Phys. Chem. B* **2000**, *104*, 3930.

(21) Anta, J A.; Nelson, J.; Quirke, N. *Phys. Rev. B* **2002**, *65*, 125324.

(22) Nelson, J.; Haque, S. A.; Klug, D. R.; Durrant, J. R. *Phys. Rev. B* **2001**, *63*, 205321.

(23) Jakobs, A.; Kehr, K. W. *Phys. Rev B* **1993**, *48*, 8780.

(24) van de Lagemaat, J.; Benkstein, K D.; Frank, A. J. *J. Phys. Chem. B* **2001**, *105*, 12433.

(25) Enright, B.; Fitzmaurice, D. *J. Phys. Chem. B* **1997**, *100*, 1027.

(26) de Jongh, P E.; Vanmaekelbergh, D. *Phys. Rev. B* **2000**, *61*, 4699.

(27) *Laboratory Techniques in Electroanalytical Chemistry*; Kissinger, T., Heinemann, W. R., Eds.; Marcel Dekker: New York, 1996; Chapter 3.

(28) Cass, M. J. Ph.D. Thesis. University of Bath, 2003

(29) Nakade, S.; Saito, Y.; Kubo, W.; Kitamura, T.; Wada, Y.; Yanagida, S. *J. Phys. Chem. B* **2003**, *107*, 14244.